# Cavity segmentation in chest radiographs

Pragnya Maduskar[1], Laurens Hogeweg[1], Helen Ayles[2], Rodney Dawson[3], Pim A. de Jong[4], Nico Karssemeijer[1], and Bram van Ginneken[1]

[1] Diagnostic Image Analysis Group, Radboud University Nijmegen Medical Centre, The Netherlands
[2] Department of Infectious and Tropical Diseases, London School of Hygiene and Tropical Medicine, London, United Kingdom
[3] University of Cape Town Lung Institute, Cape Town, South Africa
[4] Department of Radiology, University Medical Center, Utrecht, The Netherlands

**Abstract.** Cavities are air-filled spaces within a pulmonary consolidation and can be indicative of various diseases like primary bronchogenic carcinoma, mycobacterium tuberculosis, cancer and infections. Segmentation of cavities is a challenging task in chest radiographs due to the presence of superimposed structures. It is important to accurately measure the extent of cavitation to measure temporal changes and response to therapy. In this paper, we propose a semi-automatic technique for cavity border segmentation based on dynamic programming. A pixel classifier is trained using cavity border pixels based on Gaussian, location and Hessian features to construct a cavity wall likelihood map. A polar transformation of this likelihood map around the seed point is then used as a cost function to find an optimal border using dynamic programming. We have validated our technique on 50 chest radiographs (2048 $\times$ 2048 resolution, pixel size 0.25 mm, Delft Imaging Systems, The Netherlands) containing in total 50 cavities. These cavities have been manually outlined by three human experts, one chest radiologist and two readers certified to read chest radiographs according to a tuberculosis scoring system. The automatic border segmentations are compared with manual segmentations provided by the readers using Jaccard overlapping measure. The agreement between the automatically determined outlines is comparable to the inter-observer agreement.

**Keywords:** Cavity, Chest Radiograph, Tuberculosis, Segmentation

## 1 Introduction

Cavitation at the lung parenchyma is a hallmark sign of tuberculosis, a common deadly infectious disease. It is defined as a gas-filled space within a pulmonary consolidation, a mass, or a nodule, produced by the expulsion of the necrotic part of the lesion via the bronchial tree. Cavities can also occur in diseases such as primary bronchogenic carcinoma, lung cancer, pulmonary metastasis and other infections. Cavities are quite visible and distinct in CT images but are often barely visible in chest radiographs due to other superimposed 3D lung

structures in the 2D projection image. In chest radiographs, the appearance of cavities is hazy, and the cavity walls are often ill-defined or completely invisible (Fig. 2(2a)). This poses a big problem for radiologists to detect and accurately segment cavities in chest radiographs.

Assessing the size of cavity and its variation between temporal scans is important for disease diagnosis and to measure the response to therapy. Studies have shown the existence of cavitation in postprimary tuberculosis (TB) [3] which is even higher in TB patients having diabetes [5]. The number and the size of cavities is a vital element in tuberculosis scoring systems for chest radiographs [2]. Small agreement (0.55 kappa statistic) has been reported on detection of cavities in 56 chest radiographs obtained from a TB screening database [1].

Automated detection and segmentation of cavities is a less explored research area. Shen et al. [4] proposed a detection system for cavities in chest radiographs for screening of TB. Their system is based on a supervised learning approach in which candidates are segmented using a mean shift segmentation technique with adaptive thresholding for initial contour placement followed by segmentation using a snake model. Segmented candidates are then classified as cavity or non-cavity candidate using Bayesian classifier trained on gradient inverse coefficient of variation and circularity measure features. The technique was tested on only 16 cavity chest radiographs. Threshold on Tanimoto overlapping measure has been used to classify detected cavity regions as true or false positives. The accuracy of contour segmentation of cavities has not been mentioned in the work . Xu et al. [6] proposed cavity segmentation based on an improved edge-based fluid vector flow snake model. This was validated on 20 chest radiographs and resulted in a Jaccard overlapping degree of 68.8%.

In this work, we propose a dynamic programming based approach for cavity border segmentation. The center of the cavity is taken as an input to define the region of interest for dynamic programming. A pixel classifier is trained to discriminate between cavity borders and normal lung pixels using texture, Hessian and location based features constructing a cavity likelihood map. This likelihood map is then used as a cost function in polar space to find optimal path along the cavity border. The proposed technique is tested on a large cavity dataset and Jaccard overlapping measure is used to calculate the segmentation accuracy of our system.

## 2 Methods

We propose a two step method to segment the cavity borders (Fig. 1). First, a pixel classifier is trained to detect the border pixels of the cavity. Cavity border typically has a distinct fuzzy appearance on the chest radiograph (Fig. 2(1a,2a,3a)). The pixel classifier assigns each pixel a likelihood of belonging to the cavity border. This likelihood map is then used as input cost image for dynamic programming to trace the optimal path in the polar transformed image space. This constructed path corresponds to the cavity border in image space. We discuss the details of each step in the rest of the section.

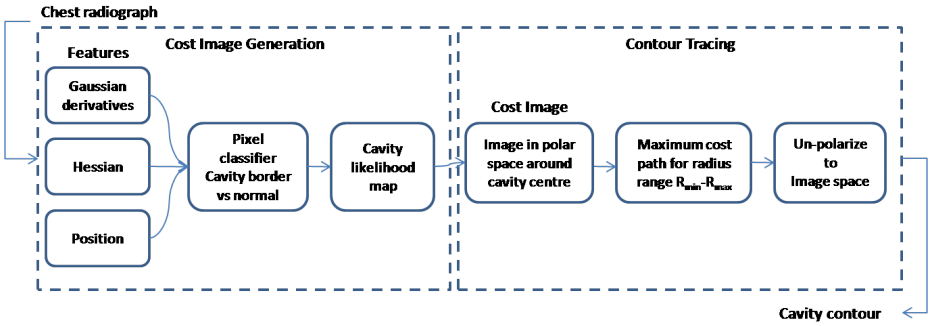


**Fig. 1.** Proposed cavity contour segmentation approach

### 2.1 Feature extraction

Various features are calculated at pixel level to capture texture, shape and location of cavity borders. The chest radiographs are subsampled by a factor of two (to 0.5 mm pixel size) to speed up feature computation process. The feature set is generated for each pixel at the subsampled level for train and test images. These pixel level features from the training set are used to train the pixel classifier, and then the classifier is applied to test images to generate a cavity border likelihood map.

**Texture features** The image is filtered with multi-scale feature bank of Gaussian derivatives to capture texture and strong edges of cavities. In chest radiographs, cavity borders give high response on higher order derivatives and this response is captured by Gaussian derivatives. The image is filtered with Gaussian derivatives of orders 0, 1, and 2 at scales $\sigma = 1, 2, 4$ pixels. In total 19 features are extracted in this step including the original intensity feature:

$I(x, y)$, pixel intensity value

$G(x, y) = \frac{1}{2\pi\sigma^2} e^{-\frac{x^2+y^2}{2\sigma^2}}$ , zero order Gaussian derivative

$G_x(x, y)$, $G_y(x, y)$ , first order Gaussian derivatives

$G_{xx}(x, y)$, $G_{xy}(x, y)$ and $G_{yy}(x, y)$, second order Gaussian derivatives

**Hessian features** Cavity walls appear like broken line segments in chest radiographs (Fig. 2(2b). This line like structure can be captured using the eigenvalues of Hessian matrix $H$ of the Gaussian filtered images. If $\lambda_1$ and $\lambda_2$ ($\mid \lambda_1 \mid \geq \mid \lambda_2 \mid$) are two eigenvalues of $H$, then $\lambda_1$ will be very large compared to $\lambda_2$ for line like structures. A total of 8 features at 4 Gaussian scales ($\sigma$) are extracted based on largest eigenvalue and ratio of eigenvalues.

**Location features** Studies have shown that cavitation mostly occurs in upper lung lobe [3]. Therefore the x and y location linearly scaled to an automatically determined bounding box around the lungs were added as features.

### 2.2 Pixel Classification

A pixel classifier is trained to assign likelihood values of being cavity border to each pixel in the chest radiographs. For the cavity border class, samples from manually annotated cavity borders are taken to train the positive class. For negative class, random samples are chosen from normal chest radiographs having no abnormalities. We have experimented with Linear Discrimant Analysis (LDA) and k-Nearest Neighbor (kNN) classifiers with and without feature selection. Similar performance was achieved with all the classifiers and feature selection did not increase the performance much due to the small feature dimensionality (29). Results for the kNN-classifier(with $k$=15) with feature normalization are reported in this paper.

### 2.3 Contour Segmentation

There are various contour segmentation methods in literature including active contour models [7], active shape models [8], and graph cut [9]. Accuracy of these techniques is highly dependent on initial contour initialization or seed point localization. Most of these methods assume the foreground object to have a uniform structure which is different from background pixels. In case of cavities, only the border is visible whereas the inside of cavity shares similar characteristics with other lung tissues due to 2D projection. To address these drawbacks, we propose a dynamic programming based solution for cavity segmentation. Given a cost image, dynamic programming can be used to find a minimum (or maximum) cost path between two pixels. Since cavities are mostly elliptical in shape, optimal path calculation is done in polar space. The polar image is constructed by extracting a circular region of interest (ROI) of radius $R$ around the seed point given as input by user. The radius $R$ is chosen sufficiently large so as to capture cavities of all sizes. In our application, we have chosen maximum radius as 50 mm. The $x$ axis in the polar image represents the angle from $-\pi$ to $\pi$ and the y axis represents the radius from 0 to $R$. Optimal cost path here refers to the maximum cost between two points since higher likelihood gives more confidence in a pixel being cavity border. We calculate cost of the optimal path at various radii starting from $R_{min}$ to $R_{max}$ with step size of $\delta_R$. For our application, we have chosen $R_{min}$ as 10 mm , $R_{max}$ as 50 mm and $\delta_R$ as 1 mm. Start and end point for the path calculation is set to the same location to ensure a closed contour when the maximum cost path is projected back to the original image space.

## 3 Dataset and Experiments

Chest radiographs for the experiment are selected from a large database of digital chest radiographs obtained from clinics in two areas of Africa with a high TB incidence. 70 images each containing a single cavity were selected from the database. Each image measured 2048 $\times$ 2048 pixels with a pixel size of 0.25 $\times$ 0.25 mm. 30 normal images were selected from the same database for training the pixel classifier. Cavity borders for the chosen 70 images have been independently marked by three human experts, one chest radiologist (referred to as the expert) and two readers certified to read chest radiographs according to the CRRS tuberculosis scoring system [2].

The pixel classifier was trained with pixels within 1 mm from manually indicated cavity borders in 20 chest radiographs as positive examples and randomly chosen pixels from 30 normal chest radiographs as negative examples. The system has been tested on the remaining 50 images and the results are compared with expert manual segmentation. We have used Jaccard overlap measure (Equation 1) for assessing the segmentation accuracy of our system. Jaccard overlap measure is also calculated between trained human readers and the chest radiologist to access inter-observer variability between human readers.

$$J(A, B) = \frac{||A \cap B||}{||A \cup B||} \tag{1}$$

## 4 Results

### 4.1 Pixel Classification

Pixel classifier results for kNN ($k = 15$) classifier are shown in Fig. 2($1b, 2b, 3b$). It can be inferred from the results that likelihood value is low for subtle cavity borders. Also the classifier occasionally responds to other structures in the radiograph, but overall, the likelihood value of the cavity border is generally higher in comparison to the surrounding tissues. This makes it possible to use this likelihood map as a cost function for dynamic programming in a sub-image to segment the cavity border.

### 4.2 Contour Segmentation

The likelihood map generated from the pixel classifier is used in polar space as cost image (Fig. 2($1c, 2c, 3c$)). Some outputs of the contour segmentation overlaid on the original image are shown in Fig. 3. The proposed technique takes 30 seconds for border segmentation of one cavity at a standard desktop PC (Core 2 Quad (Q6700)).

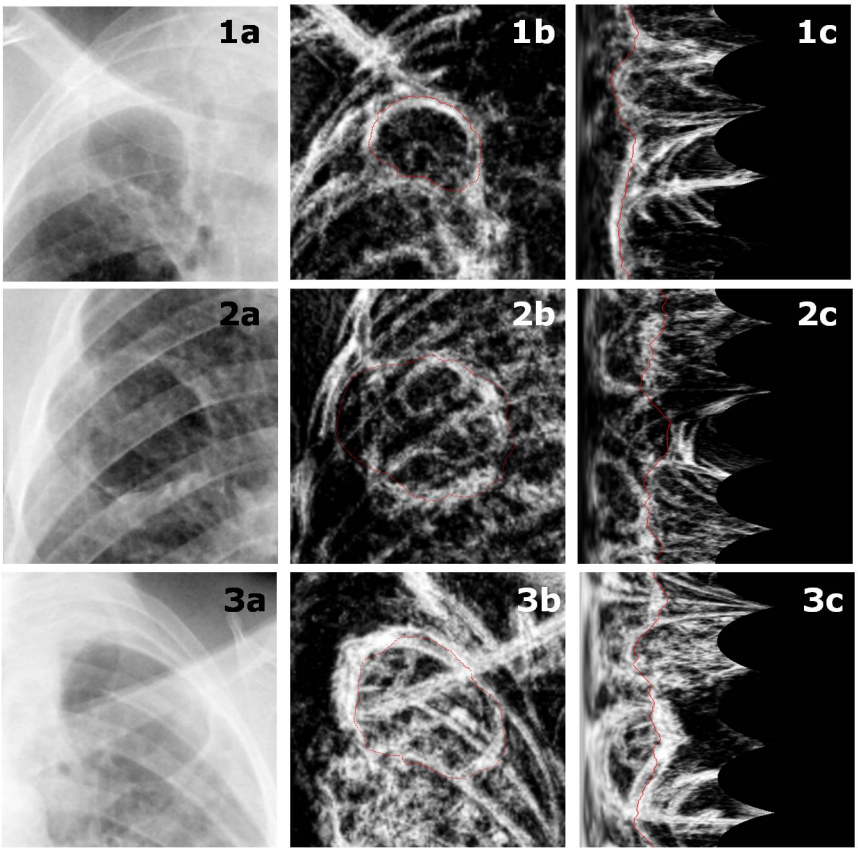


**Fig. 2.** Optimal contour path calculation. a) Original sub-image; b) Optimal path overlaid in red on the likelihood map; c) Optimal path overlaid in red on the cost image (likelihood map in polar space).

### 4.3 Quantitative assessment

Jaccard overlapping measure is calculated between Expert-Automatic computer algorithm, Expert-Reader1 and Expert-Reader2. Table 1 shows the comparison of overlap statistics between various readers and automatic segmentation. Analysis of the manual segmentations revealed that there were a substantial number of cases where the human readers exhibited large disagreement. This indicates that the delineation of cavities is a very difficult task. We therefore subdivided the test data in two groups. Set A contains 31 cavities having overlap degree greater than 0.8, referring to prominent cavities with generally clearly visible borders. Set B contains the remaining cavities (19) for which the degree of overlap was below 0.8 between readers. Our segmentation results show slightly higher degree of overlap of 0.76 for set A as compared to overall degree of overlap (0.75) for all

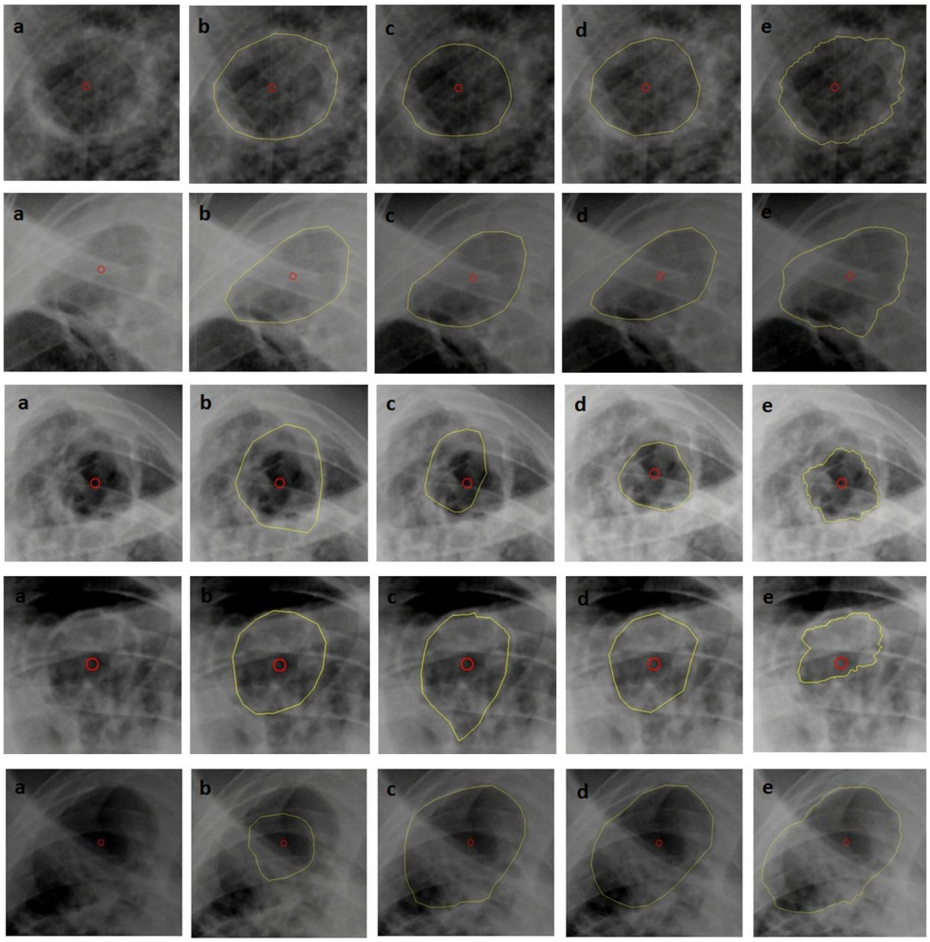


**Fig. 3.** Cavity segmentation results for five cases. a) Original sub-image; b) Expert; c) Reader1; d) Reader2; e) the automatically obtained segmentation.

the cavities. Results for set B(0.73) are comparable with the degree of overlap of manual readers(0.73 and 0.73). Overall accuracy of the proposed technique(0.75) is higher than the cavity segmentation technique presented in literature (0.69) [6].

## 5 Discussion and Conclusion

We have proposed a novel technique to automatically segment cavities based on dynamic programming which uses the likelihood map output of pixel classifier as cost function. We have validated our results with those obtained by three

| J(A,B) | Set A (31) | | | Set B (19) | | | **All (50)** | | |
|---|---|---|---|---|---|---|---|---|---|
| | $\mu$ | $\sigma$ | median | $\mu$ | $\sigma$ | median | $\boldsymbol{\mu}$ | $\boldsymbol{\sigma}$ | **median** |
| Expert-Automatic | 0.76 | 0.12 | 0.81 | 0.73 | 0.11 | 0.75 | **0.75** | **0.12** | **0.78** |
| Expert-Reader1 | 0.88 | 0.04 | 0.89 | 0.73 | 0.12 | 0.78 | **0.83** | **0.11** | **0.85** |
| Expert-Reader2 | 0.87 | 0.05 | 0.87 | 0.73 | 0.08 | 0.75 | **0.82** | **0.09** | **0.82** |

**Table 1.** Jaccard overlapping degree of segmentations for set A, set B and overall between Expert-Automatic, Expert-Reader1 and Expert-Reader2.

human expert readers on a large dataset including prominent as well as subtle cavities. Our results are very encouraging and comparable with the degree of overlap between trained human readers and a chest radiologist. Cases with low inter-observer agreement often contain subtle cavities or cavities in the diseased regions. This indicates that accurate cavity segmentation is a difficult problem.

Our work has a few limitations. In some cases the dynamic programming is attracted to rib borders. The accuracy of our technique for difficult cavities can be increased by improving the pixel classifier and optimizing the parameters for dynamic programming. It may be possible to develop pixel based features more specific to cavity borders so as to differentiate it with ribs and other bone structures. Alternatively we could include a rib suppression technique.

The dynamic programming path can be calculated more precisely if a few reference points on the contour are clicked and the path is forced to pass through those points. Providing more than one reference point can be useful for subtle cavities for precise boundary segmentation. Such a tool could be very helpful in treatment monitoring for tuberculosis.

## References


1. Abubakar, I., Story, A., Lipman, M., Bothamley, G., van Hest, R., Andrews, N., Watson, J.M., Hayward, A.: Diagnostic accuracy of digital chest radiography for pulmonary tuberculosis in a uk urban population. European Respiratory Journal 35(3), 689–692 (2010)
2. Dawson, R., Masuka, P., Edwards, D. J., Bateman, E. D., Bekker, L.-G., Wood, R., Lawn, S. D.: Chest radiograph reading and recording system: evaluation for tuberculosis screening in patients with advanced HIV. International Journal on Tuberculosis and Lung Disease 14, 52–58 (2010)
3. Koh, W., Jeong, Y.J., Kwon, J., Kim, H.J., Cho, E.H., Lew, W.J., Lee, K.S.: Chest radiographic findings in primary pulmonary tuberculosis: Observations from high school outbreaks. Korean Journal of Radiology 11, 612–617 (2010)
4. Shen, R., Cheng, I., Basu, A.: A hybrid knowledge-guided detection technique for screening of infectious pulmonary tuberculosis from chest radiographs. IEEE Transactions on Biomedical Engineering 57(11), 2646–2656 (2010)
5. Tatar, D., Senol, G., Alptekin, S., Karakurum, C., Aydin, M., Coskunol, I.: Tuberculosis in diabetics: features in an endemic area. Japanese Journal of Infectious Diseases 62(6), 423–427 (2009)
6. Xu, T., Cheng, I., Mandal, M.: An improved fluid vector flow for cavity segmentation in chest radiographs. In: International Conference on Pattern Recognition. pp. 3376–3379 (2010)

7. Kass, M., Witkin, A., Terzopoulos, D., Snakes: Active contour models, International Journal of Computer Vision, 1, 321–331 (1987)
8. Cootes, T., Taylor, C., Cooper, D., Graham, J., Active shape models–their training and application, Computer Vision and Image Understanding, 61, 38–59(1995)
9. Boykov, Y., Funka-Lea, G.:Graph Cuts and Efficient N-D Image Segmentation, International Journal of Computer Vision, 70(2) (2006)